

RESEARCH

Open Access



Challenges in Evaluating Seismic Collapse Risk for RC Buildings

Jin Zhou¹, Zhelun Zhang¹, Tessa Williams² and Sashi K. Kunnath^{1*}

Abstract

The development of fragility functions that express the probability of collapse of a building as a function of some ground motion intensity measure is an effective tool to assess seismic vulnerability of structures. However, a number of factors ranging from ground motion selection to modeling decisions can influence the quantification of collapse probability. A methodical investigation was carried out to examine the effects of component modeling and ground motion selection in establishing demand and collapse risk of a typical reinforced concrete frame building. The primary system considered in this study is a modern 6-story RC moment frame building that was designed to current code provisions in a seismically active region. Both concentrated and distributed plasticity beam–column elements were used to model the building frame and several options were considered in constitutive modeling for both options. Incremental dynamic analyses (IDA) were carried out using two suites of ground motions—the first set comprised site-dependent ground motions, while the second set was a compilation of hazard-consistent motions using the conditional scenario spectra approach. Findings from the study highlight the influence of modeling decisions and ground motion selection in the development of seismic collapse fragility functions and the characterization of risk for various demand levels.

1 Introduction

Partial or complete collapse of building structures results in casualties as well as direct and indirect economic losses following an earthquake. Because of the diverse consequences of structural collapse, many recent studies have focused on the collapse safety of buildings in high seismic zones. Collapse fragility functions, typically expressed as a function of a selected ground motion intensity measure (IM), are gaining popularity as a tool to quantify the likelihood of structural collapse during an earthquake. Haselton et al. (2011) and Liel et al. (2011) examined the collapse safety of over fifty ductile and non-ductile RC moment frame buildings through the development of fragility functions. Among other findings, their study concluded that the reduction in the minimum base

shear, introduced in ASCE 7-05 (2005) but subsequently rescinded, dramatically increases the collapse risk of long-period frame buildings in high-seismic regions. Earlier, Lee and Foutch (2002) and Jalayer (2003) assessed global dynamic instability of steel and RC frames, respectively, through the application of incremental dynamic analysis (IDA), a concept introduced originally by Bertero (1980), who suggested scaling the seismic intensity to determine capacity, but was enhanced and formalized by Vamvatsikos and Cornell (2002). The proxy for failure (which typically is a result of material degradation and geometric nonlinearities) in these studies was interstory drift (referred to as an engineering demand parameter or EDP). Ibarra and Krawinkler (2005) recognized the need to introduce some measure of the ground motion intensity into the process of establishing collapse capacity. They proposed a methodology for collapse assessment using the ratio of ground motion intensity, such as spectral acceleration at the first mode period, $S_a(T_1)$, to

*Correspondence: skkunnath@ucdavis.edu

¹ Civil and Environmental Engineering, University of California, Davis, CA 95616, USA

Full list of author information is available at the end of the article
Journal information: ISSN 1976-0485 / eISSN 2234-1315

a structural strength parameter (normalized base shear capacity).

Fragility functions are typically predicated on a ground motion IM, such as peak ground acceleration (PGA) or spectral acceleration at a given period. As discussed in Luco and Cornell (2007), the selection of an appropriate IM is driven by its “efficiency” and “sufficiency,” both of which are characteristics tied to the accuracy of probabilistic seismic demand prediction. An efficient IM should result in a relatively small variability of the structural demand measure given IM, and a sufficient IM should render the selected demand measure to be conditionally independent of earthquake magnitude and source-to-site distance. Of the many possible choices for IM, $S_a(T_1)$ has been shown to meet the criteria of efficiency and sufficiency for first-mode dominated buildings (Shome et al. 1998). Enhanced intensity measures would be needed for taller buildings, where higher modes contribute significantly to the system response.

One of the issues that emerges from past research on collapse assessment is that a number of factors influences the quantification of collapse probability. These factors range from the analysis approach to modeling considerations at the component and material level to ground motion selection and the choice of intensity measures. Likewise, nonlinear analysis of a structure to generate the response data can be carried out using different approaches. Typically, buildings are modeled using frame elements with concentrated or distributed plasticity. While the former is computationally more efficient, it has several drawbacks, such as the need to predetermine sectional properties and its inability to consider axial force—bending moment (P–M) interaction. Distributed plasticity elements, on the other hand, can simulate the spread of plasticity and incorporate P–M interaction. Previous studies have employed both approaches: Haselton et al. (2011) and Liel et al. (2011) utilized concentrated springs at the ends of elastic beam–columns, whereas distributed plasticity elements with fiber-section models were used in the assessments reported in Rajeev and Tesfamariam (2012) and Koopae et al. (2015). It has been shown by Koopae et al. (2015) that the response is sensitive to the choice of constitutive models used in the nonlinear simulation, thus leading to different collapse capacity predictions. Nonlinear dynamic techniques, such as IDA and Multi-Stripe Analysis (MSA) which is discussed in Jalayer and Cornell (2009) are based on time history analysis. Thus, the selection of GMs used in the study plays a significant role in the collapse predictions. The suites of GMs used in the simulations must be adequate to provide reliable statistical results to generate a fragility function. For example, Koopae et al. (2017) used different GM selection methods and demonstrated

that the predicted collapse fragilities were affected by the GM selection method as well as the choice of structural period in anchoring the IM.

Based on the aforementioned issues, a systematic investigation was carried out to examine the effects of modeling considerations and GM selection in establishing collapse fragility functions of typical RC buildings in the context of assessing the risk of exceeding a particular drift demand. Collapse fragilities only provide a relationship between collapse probability and a selected intensity measure. In the present study, we extend the relationship to include the rate of occurrence of the ground motions, thereby enabling the quantification of “demand risk” that provides the return period of a certain demand level on the building. The demand risk plots can be used to estimate the risk of a range of demand levels—from design-level drifts to extreme drifts that signal imminent collapse. The primary system considered in this study is a seismically detailed 6-story RC moment frame building as per current ASCE/SEI 7-16 (2016) requirements. Both distributed and concentrated plasticity beam–column elements were used to model the building frame and several options were considered in constitutive modeling for both options. Finally, fragility functions and EDP risk are compared for different modeling assumptions using two GM selection methods.

2 Description of Selected Building

The building selected for the comparative evaluation was designed for a site in northern California in accordance with the requirements of ASCE/SEI 7-16 (2016) and ACI 318-14 (2014). The following spectral values were used to establish the design base shear: $S_s = 1.715g$ and $S_1 = 0.792g$. The resulting design spectrum at the site is shown later in Sect. 4 that describes the ground motion selection process. The plan view and typical elevation of the building are shown in Fig. 1. Additional design information, including section sizes and reinforcing details, are provided in Table 1. The perimeter frames support the entire seismic lateral forces, and the interior frames are designed to carry only gravity loads. The building is symmetric in the plan; hence, only a typical perimeter frame was considered in the analysis. The base of the building is assumed to be fixed (fully restrained). An eigenvalue analysis of the building model indicates the following modal periods: $T_1 = 1.0s$, $T_2 = 0.35s$.

3 Modeling Considerations

Two-dimensional frame models were developed using the OpenSees (2019) platform. Members were modeled using two approaches: force-based beam–columns with fiber sections at five Gauss–Lobatto integration points

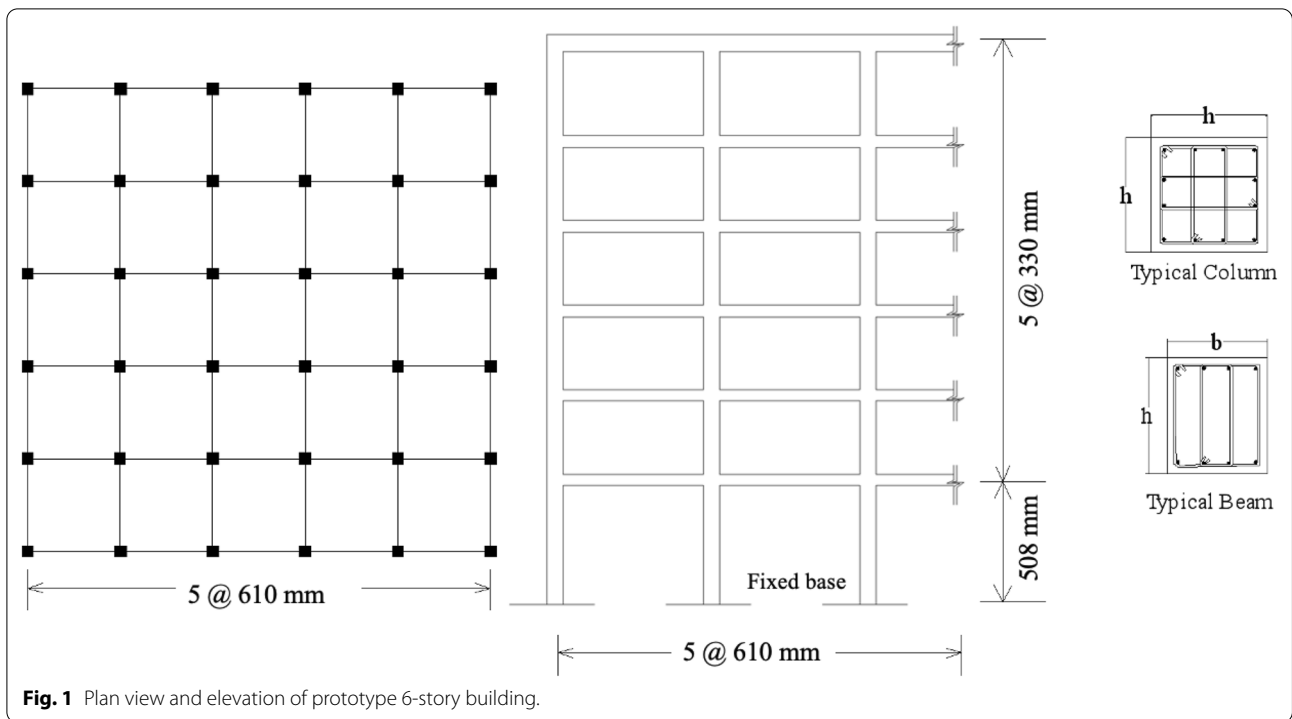


Table 1 Section and reinforcement details.

Floor	Beams			Columns			
	Size, $b \times h$ (mm)	Long reinf.		Trans reinf.	Size, h (mm)	Long reinf.	Trans reinf.
		Bot	Top				
1–2	610 × 762	9 ϕ 29	10 ϕ 29	ϕ 13 @ 127	762	20 ϕ 36	ϕ 13 @ 127
3–4	559 × 711	8 ϕ 29	10 ϕ 29	ϕ 13 @ 127	711	16 ϕ 36	ϕ 13 @ 127
5–6	508 × 610	5 ϕ 29	7 ϕ 29	ϕ 13 @ 127	610	16 ϕ 29	ϕ 13 @ 127

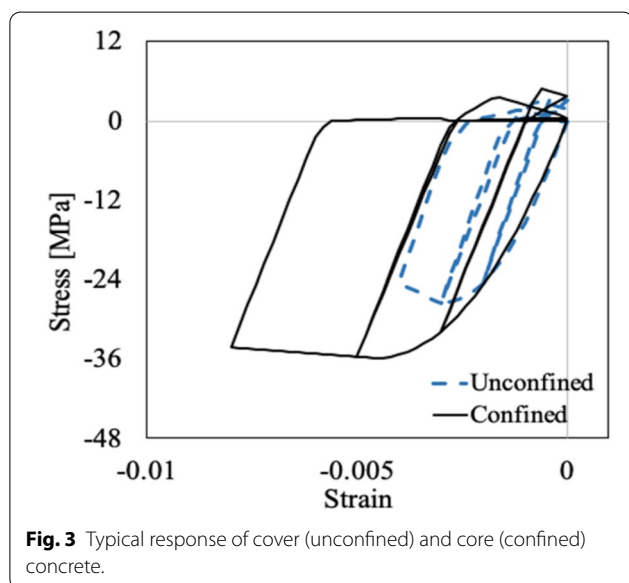
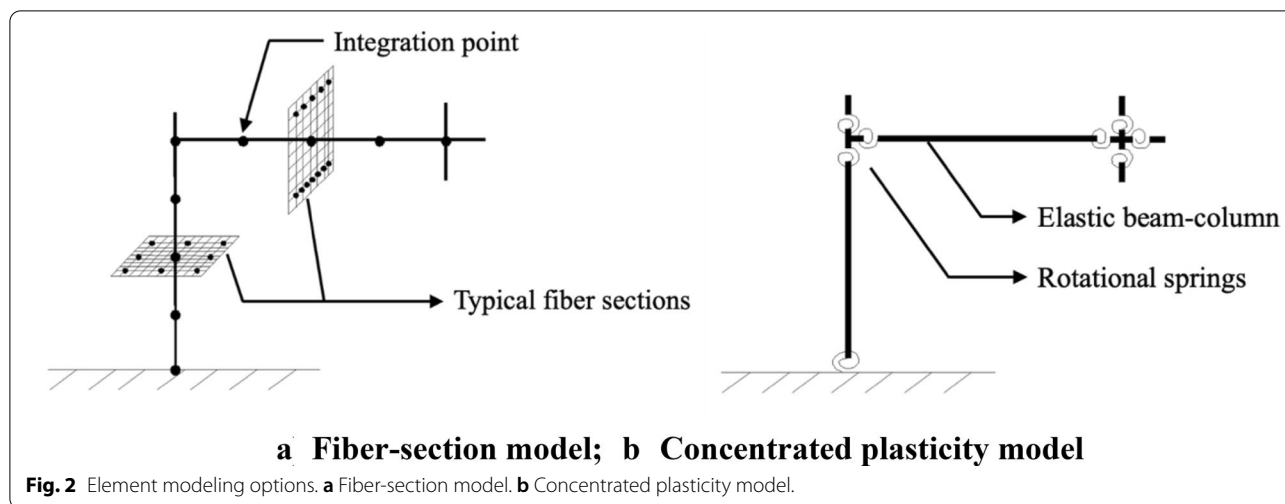
Notation: ϕ = bar diameter (all dimensions in mm).

along the member length; and concentrated plastic hinges at the ends of the element connected in series to elastic beam–columns. The co-rotational geometric transformation was invoked in OpenSees to handle large deformations. It is acknowledged that localization in distributed plasticity elements can be an issue when the deformations enter the post-peak softening phase—limiting the force-based element to five integration points controls the localization phenomenon to a significant degree. The nonlinear dynamic analysis was performed using the Newmark-beta constant average acceleration integration scheme and Rayleigh damping was specified with 5% viscous damping in modes 1 and 6. To avoid spurious damping forces in the inelastic

range, stiffness-proportional damping is constructed using the tangent stiffness matrix, a feature available in OpenSees.

3.1 Component and Material Modeling

Frame elements were modeled using two options: (a) fiber-section models and (b) concentrated inelastic springs. A partial section of the building frame with typical fibers in a beam and column is illustrated in Fig. 2a. In the second approach, the structure is modeled using elastic beam–column elements with rotational springs to represent the structure’s nonlinear behavior at the ends of each element, as shown in Fig. 2b and the elastic element is connected in series to the rotational spring.

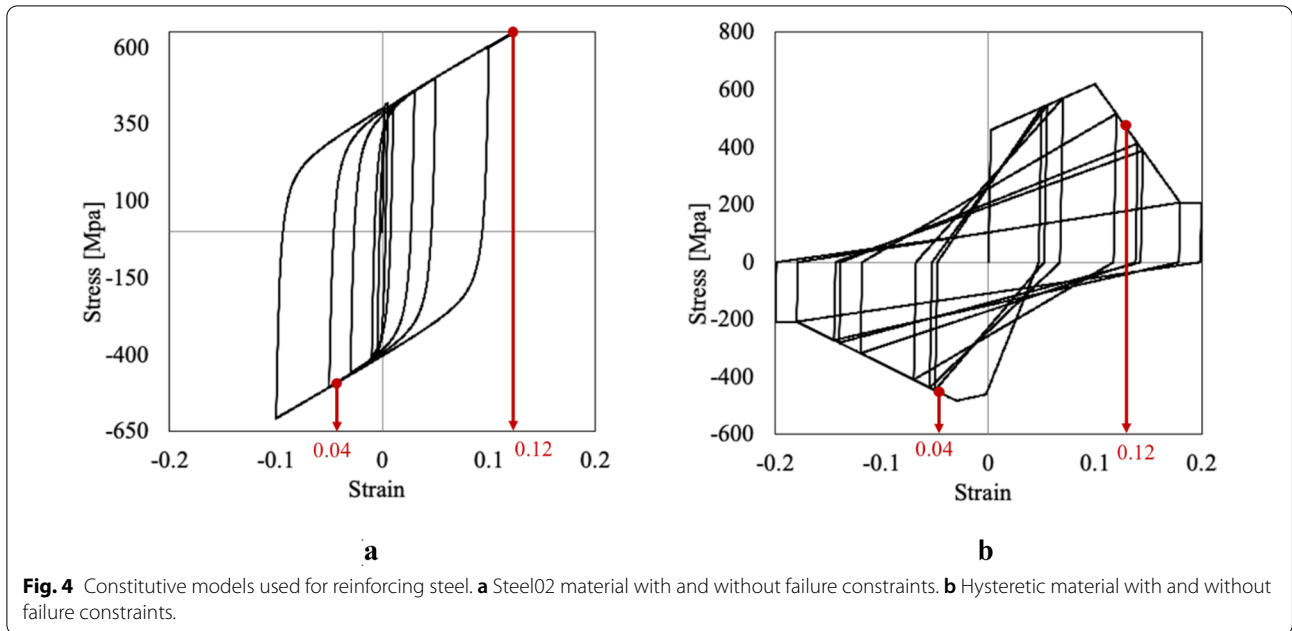


In the case of fiber-section modeling, the modified Kent–Park model (Scott et al. 1982) was adopted to determine the properties of the confined concrete. The material model in OpenSees used to define concrete fibers is the “Concrete02” material which is based on the model developed by Yassin (1994) and consists of a nonlinear curve in compression and linear elastic behavior in tension up to tension cracking followed by linear softening. Typical monotonic and cyclic responses of both unconfined and confined concrete are shown in Fig. 3.

Two methods are used to simulate the behavior of reinforcing steel: in the first approach (referred to as Model FS02), the steel reinforcing bars are modeled

using the “Steel02” material in OpenSees, which constructs a uniaxial Giuffre–Menegotto–Pinto steel material with isotropic strain hardening (Menegotto & Pinto, 1972); in the second approach, (denoted by Model FHYS), the “Hysteretic” material in OpenSees is used, so that softening behavior could be specified beyond the ultimate stress, because the post-peak response of structural components has been shown to significantly affect the predicted collapse capacity of structures (Ibarra & Krawinkler, 2005). Softening on the tension side signifies necking of the bar leading to rupture, whereas on the compression side, it represents the initiation of bar buckling. In addition to these two variations in modeling the reinforcing steel, an additional consideration was incorporated to represent material failure. In OpenSees, a fiber can be indirectly removed (or attain a failure limit state) by specifying capping strains in compression and tension through the “MinMax” material object. Particularly for the Steel02 material, that continues to harden without bounds, this option provides a simple and convenient method to limit the capacity of a section when the material model does not allow for post-peak softening. The “MinMax” constraint was applied to both Steel02 and Hysteretic materials and are denoted by FS02-M and FHYS-M, respectively.

A preliminary IDA was carried out using several ground motions and the peak strains in tension and compression were recorded at the collapse limit state. Based on average observed strains in the reinforcing steel at collapse, the tensile failure strain was set at 12% and failure due to buckling in compression was specified as 4%. The MinMax material returns zero stresses when the fiber strains exceed these values. The cyclic



response of the materials, including assumed values of the capping strains, are shown in Fig. 4.

3.2 Moment–Rotation Model for Rotational Springs

In the case of rotational springs, the moment–rotation behavior needs to be specified at the start of the analysis. In the present study, the sectional moment–curvature response of each cross section was first obtained. The yield moment of the section was defined at the first yield of a longitudinal bar. Assuming a linear curvature profile up to yield, the corresponding rotation is directly obtained through integration of the curvature profile across the length. Beyond the yield

limit, curvatures were converted into rotation using an assumed plastic hinge length:

$$\theta_i = (\phi_i - \phi_y)l_p, \tag{1}$$

where θ_i is the rotation at step i , ϕ_i is the computed curvature at the same step and l_p is the plastic hinge length, assumed to be equal to half the depth of the section. The resulting moment–rotation response was then idealized into a trilinear curve, as shown in Fig. 5a. Once the monotonic moment–rotation relationship was established using this procedure, the cyclic behavior of the rotational spring was specified using the Hysteretic material (denoted hereafter as Model SPR), as shown in

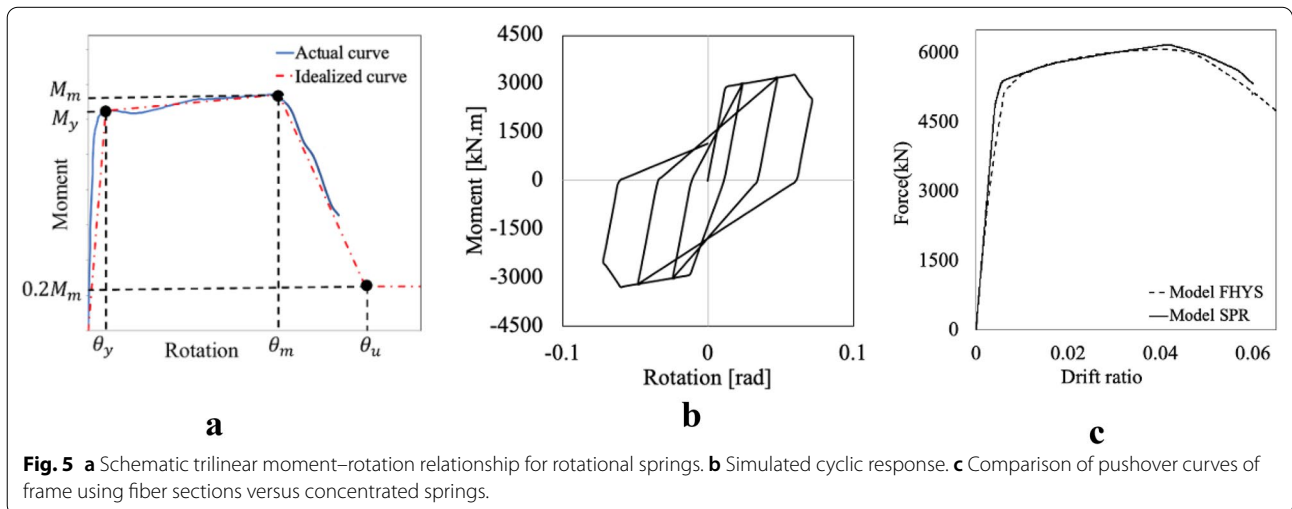


Fig. 5b. Since the building being evaluated is a modern ductile moment frame, no deterioration in stiffness or strength was specified. The effect of this assumption was determined (through comparisons of the GM intensity at the target 6% inter-story drift used to quantify imminent collapse) to be not significant, since the post-peak softening behavior was more critical at the collapse limit state. The calibration of the concentrated plastic hinges using the above methodology was verified in two ways: first the modal periods of the frame using the two approaches were shown to be nearly identical; and secondly, the pushover responses of the two frame modeling schemes were compared (see Fig. 5c).

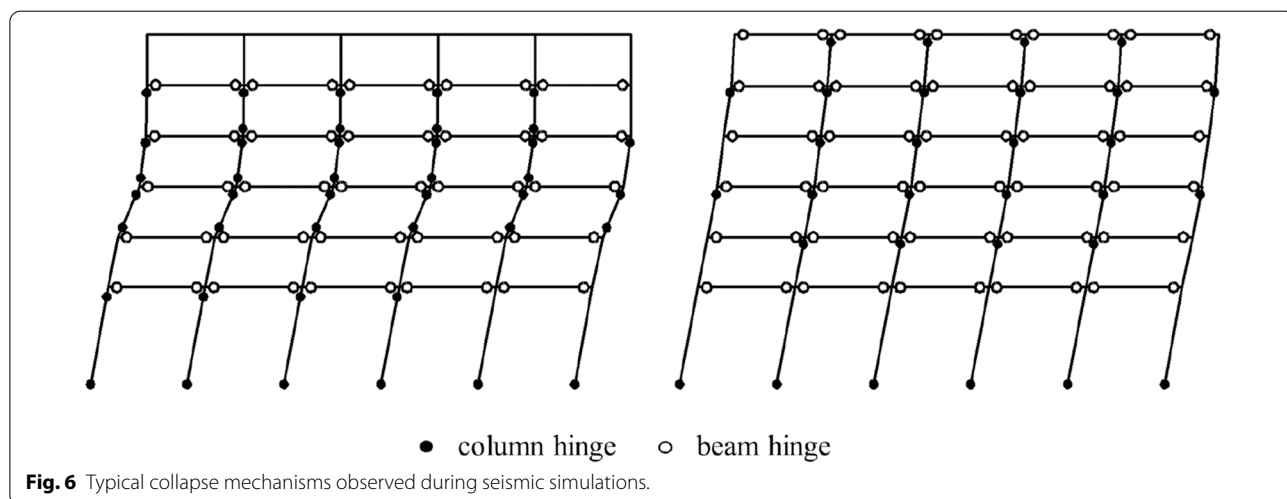
Finally, as with the previous modeling choices, an additional option was considered for the model with concentrated springs: peak rotations were capped by invoking the MinMax material object and this is denoted in the study as Model SPR-M. To establish the capping rotations, maximum rotational deformations in the springs were monitored at the collapse limit state. Consequently, the limiting rotations used to define a collapse condition were $\pm 6\%$. A summary of the different models considered in the study is presented in Table 2.

3.3 Building Collapse Criterion

In IDA, collapse is defined as the point of dynamic instability, where the lateral story drifts of the building increase without bounds. This typically occurs when the IDA curve becomes nearly flat. In the present study, the so-called flat-lining of the IDA curve was not evident in several of the simulations. Hence, the definition of collapse was further validated by not automatically assuming that non-convergence represents collapse but actually assessing whether a collapse mechanism has formed. To ensure that a collapse condition was reached, the hinge mechanism at peak interstory drift was examined. Figure 6 shows two examples of peak interstory drifts leading to a local story or global collapse mechanism. Based on a comprehensive assessment of both the impending collapse mechanisms and the near flat-lining of the IDA curve leading to non-convergence, a peak interstory drift ratio of 6% was used to classify a collapse state. This magnitude is also consistent with the interstory drift ratio (IDR) attained after the post-peak softening observed in the pushover curve (shown previously in Fig. 5c) as well as collapse drifts reported in previous studies (i.e., Haselton et al. report collapse drifts ranging from 5 to 8%).

Table 2 Summary of models used in study.

Model	Beam-column element type	Description
FS02	Fiber section	Steel reinforcing bars are modeled using the “Steel02” material in OpenSees
FS02-M		Model FS02 described is enhanced with failure constraints
FHYS		Reinforcing bars are modeled using the “Hysteretic” material in OpenSees
FHYS-M		Failure constraints are added to the above-referenced FHYS model
SPR	Concentrated plasticity	The sectional response is simulated using rotational springs
SPR-M		Failure constraints are added to the rotational springs defined above

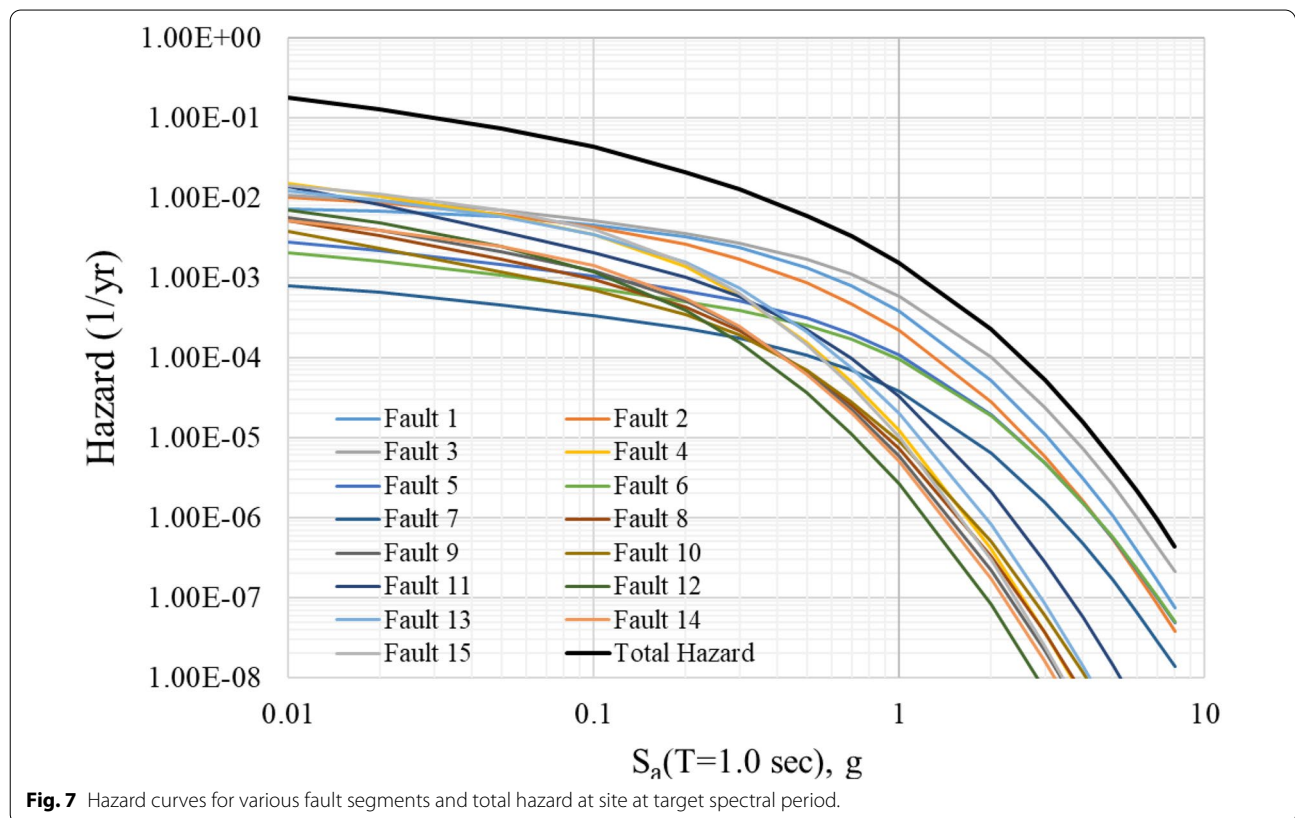


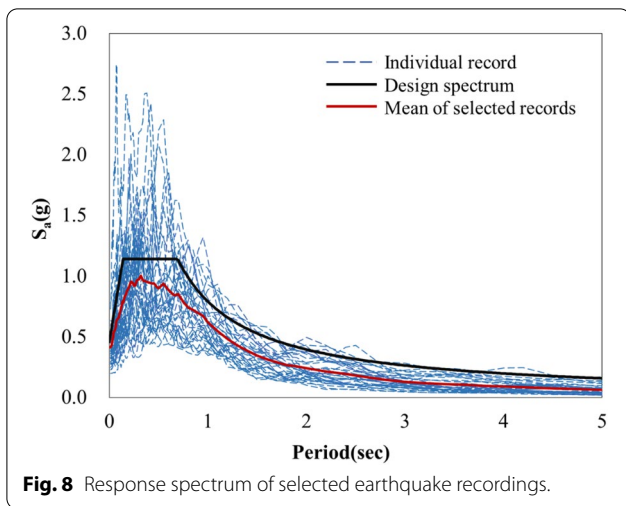
4 Ground Motion Selection

Based on the building location, the primary sources contributing to the seismic hazard are the Hayward, Rodgers Creek, San Andreas, Calaveras, Concord, Greenville and San Gregorio faults. A site-specific probabilistic seismic hazard analysis (PSHA) was initially conducted to generate the uniform hazard spectra (UHS) for a range of ground-motion hazard levels. The hazard deaggregation provides the fractional contribution of different scenario pairs (earthquake magnitude and distance) to the total hazard. For the selected building site, the hazard corresponding to a 2% probability of exceedance in 50 years is generally controlled by seismicity on the Hayward Fault with a mean magnitude (M_{bar}) of 6.9 and a mean rupture distance (R_{bar}) of ~ 2 km. The hazard at this site is also affected by scenarios from the Rodgers Creek Fault (M_{bar} of 7.1 and R_{bar} of 3 km), the San Andreas Fault (M_{bar} of 8.0 and R_{bar} of 28 km), and the Calaveras Fault (M_{bar} of 6.9 and R_{bar} of 22 km). Figure 7 shows the various hazard curves for 15 different fault segments as well as the total hazard at the site corresponding to the target spectral acceleration $S_a(T = 1.0 \text{ s})$.

4.1 GM Set 1—Site-Specific Motions for IDA Study

Using site-specific criteria identified in the previous section and specifying soil sites with average shear wave velocity (V_{s30}) 200–400 m/s (corresponding to site class D), an initial suite of 100 ground motions were extracted from the PEER Strong Motion database (<https://ngawest2.berkeley.edu/>) for the IDA study. The selected motions included both non-pulse and pulse-like motions. Based on the rupture distance of ~ 2 km from the main causative fault (Hayward) and a total epsilon of 1 (corresponding to the design spectrum per ASCE/SEI 7-16), Hayden et al. (2014) recommend that the proportion of pulse motions should be approximately 80 percent. Consequently, the final set of 50 motions used in the IDA study consisted of 40 pulse-like motions. The process of eliminating records from the initial selection was dictated by the degree of scaling that would be needed during the generation of the IDA curves. If the $S_a(T_1)$ of an unscaled record is very low, then a very large scale factor would be needed to reach the collapse IM. As pointed out by Baker and Cornell (2005), scaling low-to-moderate-IM ground motions up to extreme-IM levels is not an appropriate way to represent shaking associated with real occurrences of such large-IM levels. In addition, Davalos and Miranda (2019) show that excessive scaling can also lead





to bias in the estimated collapse probability. Therefore, selected records with the lowest $S_a(T_1)$ values were discarded and only the highest 50 were retained. Examining the final selection of GMs, the actual magnitude range of the selected accelerograms is between 5.4 and 7.6 and the fault distance varies from 2 to 22 km. Figure 8 shows the spectra of the individual records as well as the ASCE/SEI 7-16 design response spectrum and the mean spectrum of the selected records are also superimposed in the same figure.

4.2 GM Set 2—Hazard-Consistent GM Selection Using Conditional Scenario Spectra

The ground motions selected for generating the IDA curves (GM Set 1) are site-specific but not hazard

consistent—meaning that the spectra of the selected motions do not have rates of occurrence that reproduce the hazard at the site in terms of both the hazard levels and period range of interest.

Hence, an alternate approach was used based on the conditional scenario spectra (CSS) methodology proposed by Arteta and Abrahamson (2019), which results in a set of earthquake time series each with a scale factor and rate of occurrence such that the ground-motion hazard is fully captured by the time series. The UHS were used to compute conditional mean spectra (CMS) for each hazard level using the procedure outlined in Baker (2011), as follows:

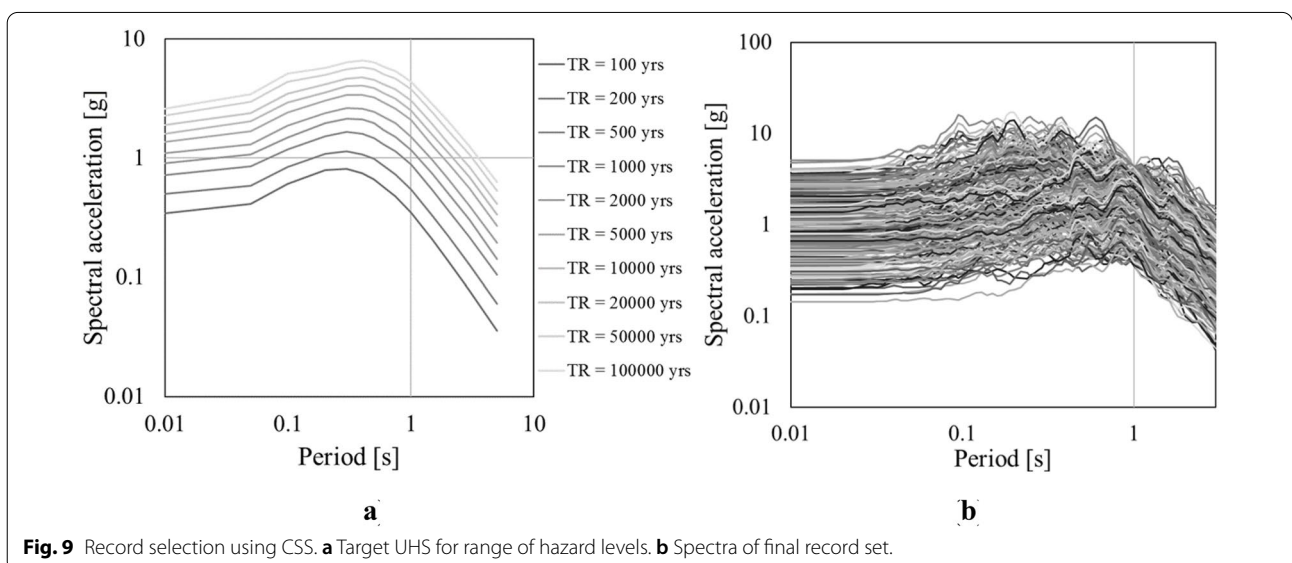
$$\ln(\text{CMS}(T)) = \ln(\text{SA}_{\text{med}}(T)) + \varepsilon_{\text{bar}}(T)\sigma(T), \quad (2)$$

$$\varepsilon_{\text{bar}}(T) = \varepsilon^*(T)\rho(T, T_0), \quad (3)$$

where $\text{CMS}(T)$ is the S_a value of the *CMS* at period T , SA_{med} is the median S_a computed from the controlling scenario for each hazard level, $\varepsilon_{\text{bar}}(T)$ is the mean epsilon at period T , $\varepsilon^*(T)$ is the number of standard deviations required to reach the UHS at the conditioning period T_0 , and $\rho(T, T_0)$ is the correlation between $\varepsilon(T)$ and $\varepsilon(T_0)$. In this study, each CMS was conditioned at a period of 1.0 s, the fundamental period of the building. The variability about each CMS, known as the conditional spectrum (CS), was computed using

$$\sigma_{\text{CS}}(T) = \sigma_{\text{medSA}}(T)\sqrt{(1 - \rho^2(T, T_0))}, \quad (4)$$

where $\sigma_{\text{CS}}(T)$ is the conditional standard deviation at period T , $\sigma_{\text{medSA}}(T)$ is the standard deviation of the S_a at period T estimated from the ground-motion model. The



conditional standard deviation combined with the CMS describes the complete distribution of the S_a values at each period (Lin & Baker, 2015). Figure 9a shows the target UHS used in the analysis for ten hazard levels with annual rates of exceedance ranging from 10^{-2} to 10^{-5} .

An initial set of time series was selected based on the PSHA deaggregation results. A subset of earthquake time series was then selected based on spectral shape so that the CMS and variability about the CMS (the CS) were recaptured by the time series at each hazard level. The initial rate of occurrence was estimated for each time history by subtracting neighboring hazard levels ($HAZLevel_i$ and $HAZLevel_{i+1}$) and dividing by the number of time histories (N) that fall between the two hazard levels at the conditioning period, as indicated in Eq. (6) below:

$$Rate_{TH,i} = \frac{HAZLevel_i - HAZLevel_{i+1}}{N} \tag{5}$$

The rates were then adjusted iteratively so that the hazard was recaptured by the set of scaled time histories, resulting in a final set of hazard-consistent time histories, known as the CSS. Complete details on the methodology are reported in Arteta and Abrahamson (2019). Application of the CSS approach resulted in the selection of 33 unique time series which were scaled to fall between the specified hazard levels at the conditioning period. This produced a total of 297 ground-motion sets [note that the mid-point between 2 consecutive UHS spectra is used at the selected conditioning period to compute the CMS, thereby resulting in $33*(N - 1)$ time series], each with an assigned rate of occurrence, such that the UHS at each hazard level was recaptured by the scaled earthquake records—only one of the horizontal components is used in the present study. The spectra of the final CSS set is shown in Fig. 9b. To develop fragility curves for the

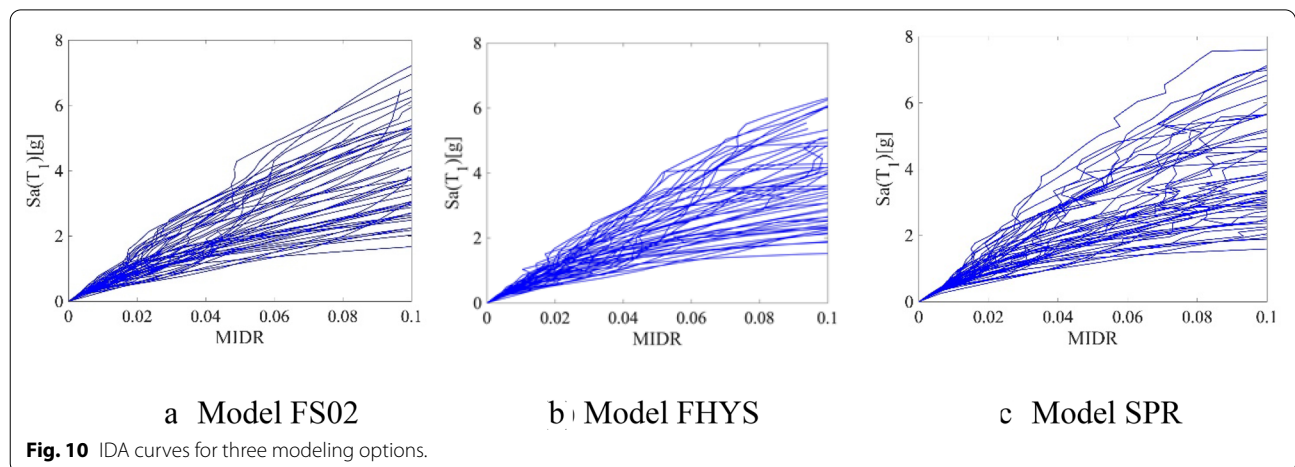
CSS approach, each time history was weighted by the rate of occurrence, which is discussed later in this paper.

5 Nonlinear Seismic Simulations

Nonlinear simulations using OpenSees were carried out on the six separate models of the 6-story frame, i.e., models FS02, FS-02-M, FHYS, FHYS-M, SPR and SPR-M as previously described. For the IDA study, seismic simulations are carried out at increasing intensities until a collapse condition, as defined in Sect. 3.3 is attained. Simulations were performed using the suite of 50 ground motions from GM Set 1 to generate 50 IDA curves. Figure 10 displays the IDA curves obtained for three different modeling options. While some IDA curves terminated at much larger drifts, the plots are truncated at 10% and the IM values are determined at the collapse condition corresponding to 6% maximum inter-story drift ratio (MIDR)—this typically involves interpolating between two IM values. Unlike IDA, GM selection using the CSS methodology results in a large ensemble of records that cover a range of intensities as discussed in Sect. 4.2. The seismic demands resulting from CSS are shown in Fig. 11, where each point represents the maximum interstory drift ratio for each ground motion. MIDRs equal to or exceeding 6% are all shown at the collapse limit of 6%.

6 Collapse Fragility Functions—Effect of Modeling Considerations

Seismic demands, in general, and structure-specific collapse drifts, in particular, are highly record dependent. This record-to-record (RTR) variability is usually accounted for if the fragility function is developed from a reasonably large set of records. Previous studies that have been cited in this paper suggest a number equal to or larger than 30 to be adequate to incorporate RTR



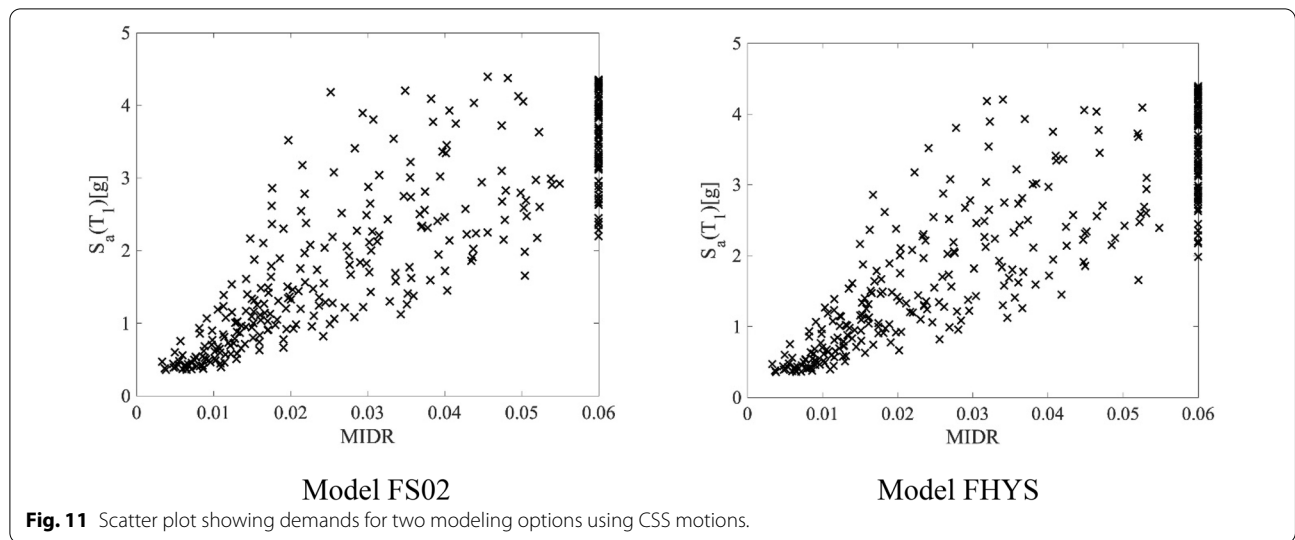


Fig. 11 Scatter plot showing demands for two modeling options using CSS motions.

Table 3 Amplitude range of $S_a(T_1)$ in each bin.

Bin	1	2	3	4	5	6	7	8	9	10
S_{a_i} (g)	0.0	0.5	1.3	1.7	2.1	2.6	3.2	4.0	5.4	6.0
$S_{a_{i+1}}$ (g)	0.5	1.3	1.7	2.1	2.6	3.2	4.0	5.4	6.0	6.0+

variability. Matching the mean of the spectral shapes of the selected records to the design spectrum also aids in minimizing the effects of RTR variability (Iervolino et al., 2008). In the present study, the dispersion of the IM of the selected records is incorporated into the statistical fitting of the observed data, hence RTR variability is explicitly considered. It is well-acknowledged that a log-normal distribution, which is characterized by the median and standard deviation of the natural logarithm of the IMs, yields the best representation of the distribution of any damage state in the framework of performance-based seismic assessment of structures (Ibarra & Krawinkler, 2011; Shome & Cornell, 1999, among others). The lognormal cumulative distribution function used to develop the fragility functions presented in this paper can be expressed as

$$P(C|IM = x) = \Phi\left(\frac{\ln(x/\theta)}{\beta}\right), \tag{6}$$

where $P(C|IM = x)$ is the probability of collapse of the structure under the ground motion with $IM = x$, $\Phi()$ is the standard normal cumulative distribution function, θ is the median of the fragility function (i.e., the IM magnitude that corresponds to 50% probability of collapse) and β is the standard deviation of $\ln(IM)$.

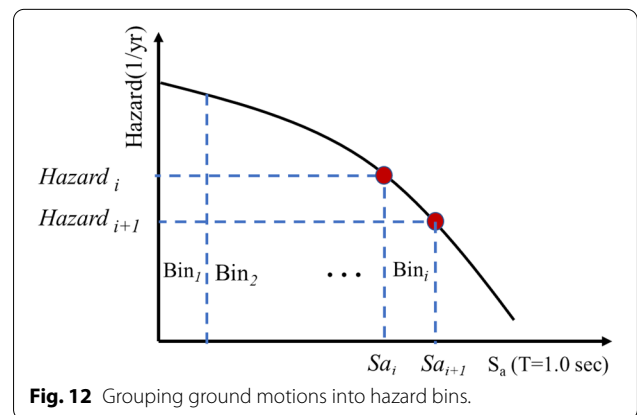


Fig. 12 Grouping ground motions into hazard bins.

The IDA curves presented in Fig. 10 produce a set of IM values associated with the onset of collapse for each ground motion (GM). Since one of the primary objectives of the study is to assess the risk associated with an EDP (maximum interstory drift in this study), the GMs are grouped into bins based on S_a ranges, as shown in Table 3. The associated hazards in a typical Bin ‘i’ is shown conceptually in Fig. 12. The rate of the GMs in any bin ‘i’, $Rate_{bin,i}$, is obtained from

$$Rate_{bin,i} = \frac{Hazard_i - Hazard_{i+1}}{ngm_i}, \tag{7}$$

where ngm_i is the number of ground motions in bin ‘ i ’. The total hazard curve shown previously in Fig. 7 is used to obtain the hazard data in Eq. (8). Following the non-linear simulations of the building model at increasing intensity levels, the number of collapse cases in each bin is counted. Unlike the hazard-consistent CSS approach, where the GMs in a particular bin have different rates, GMs in each bin using GM Set 1 have the same rate. Based on the fraction of events that cause collapse, the discrete collapse probability in each bin can be evaluated as follows:

$$P(C|S_{a_i} = \bar{S}_{a_i}) = \frac{\sum_{j=1}^{ngm_i} H(MIDR_{i,j} - d_c)}{ngm_i} \quad (8)$$

In the above expression, $P(C|S_{a_i} = \bar{S}_{a_i})$ is the collapse probability for the hazard level corresponding to \bar{S}_{a_i} , where \bar{S}_{a_i} = mean $S_a(T_1)$ of GMs in bin i , $MIDR_{i,j}$ is the maximum interstory drift ratio of GM j in bin i and $H(MIDR_{i,j} - d_c)$ is the Heaviside function that assumes a value of 0 or 1 depending on whether the MIDR exceeds the collapse drift d_c . A sample set of results using the process described above and applying Eq. (9) to the IDA curves shown in Fig. 10 (for Model FS02) is shown in Fig. 13.

Collapse fragility functions were subsequently developed from the IDA curves for each of the material modeling options presented in Sects. 3.1 and 3.2. The collapse probability plots are displayed in Fig. 14 for ground motions from GM Set 1, where it is evident that modeling choices do not have a significant impact on

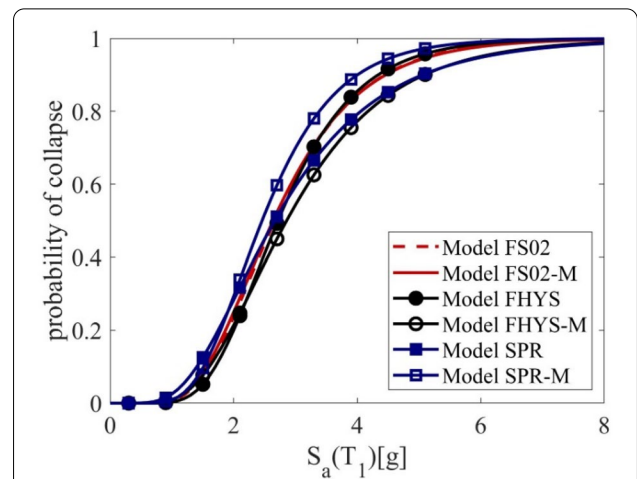


Fig. 14 Collapse fragility functions for all modeling choices based on IDA and GM Set 1.

the predicted median collapse probabilities. The biggest discrepancy occurs between models SPR-M and FHYS-M with intensity levels for the median collapse probability varying approximately between $S_a = 2.5$ g to $S_a = 2.85$ g. Part of the reason for the limited variability between modeling options is likely due to the fact that the GM set is dominated by pulse-like motions, where the peak story drift is controlled by a single large inelastic cycle. Specifying limiting deformations that signify material failure (either strain for the fiber-section models or rotation for the spring models) increases the median collapse probability for the concentrated plasticity model only.

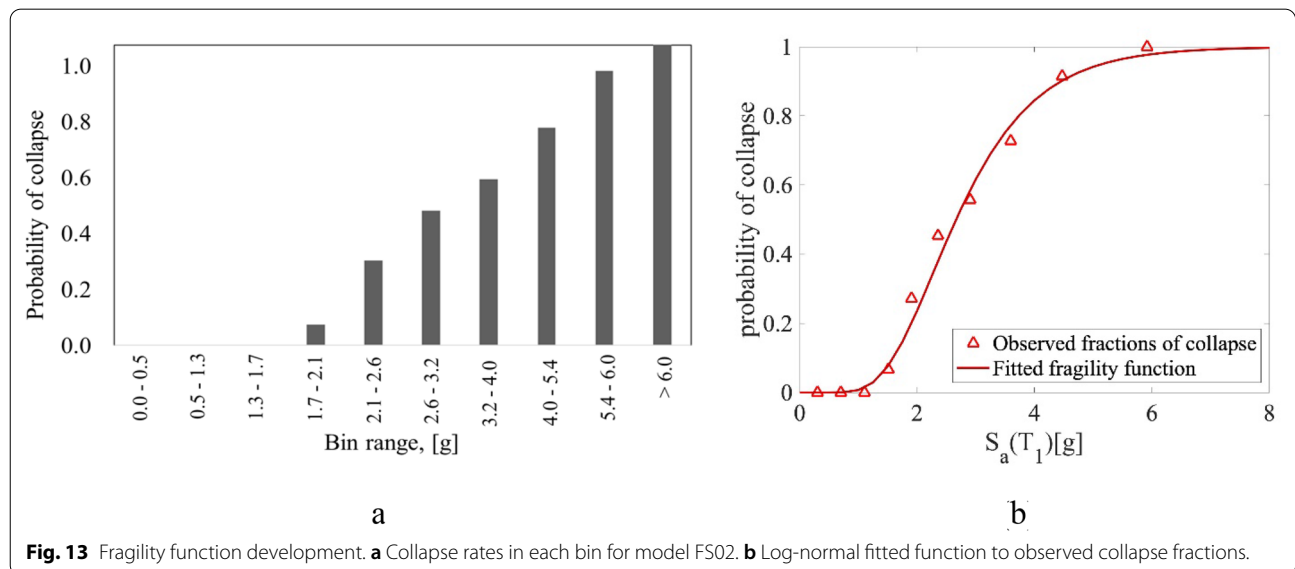


Fig. 13 Fragility function development. a Collapse rates in each bin for model FS02. b Log-normal fitted function to observed collapse fractions.

6.1 Fragility Functions Using Hazard-Consistent Ground Motions (GM Set 2)

To develop hazard-consistent fragility curves, the probability of collapse from each time history was weighted by the time series rate of occurrence, which was selected and adjusted as previously discussed in Sect. 4.2. Therefore, generating fragility functions from the CSS simulations shown in Fig. 11 requires that the data first be sorted into appropriate bins consistent with the hazard (i.e., return period). After the GMs are grouped into their hazard-consistent bins, the number of collapse cases in each bin is established. Based on the fraction of events that cause collapse, we can estimate the discrete probability for each hazard level, as follows:

$$P(C|Haz = k) = \sum_{m=1}^{ngm} Haz_{frac,m} H(MIDR - d_c), \tag{9}$$

$$\text{where } Haz_{frac,m} = \frac{RateGM_m}{\sum_{m=1}^{ngm} RateGM_m}. \tag{10}$$

In the above expression, $P(C|Haz = k)$ is the collapse probability for hazard level $Haz = k$, ngm is the number of unique GMs used in the assessment (33 in this study), $Haz_{frac,m}$ is the fractional contribution of GM_m to the total hazard for Hazard Level k , $RateGM_m$ is the rate associated with GM_m , and $H(MIDR - d_c)$ is the Heaviside function that assumes a value of 0 or 1 depending on whether the MIDR exceeds the collapse drift d_c . The resulting discrete probability distribution for one modeling option (SPR-M) is shown in Fig. 15a and the corresponding log-normal fitted fragility function is shown in Fig. 15b. This procedure was then applied to all

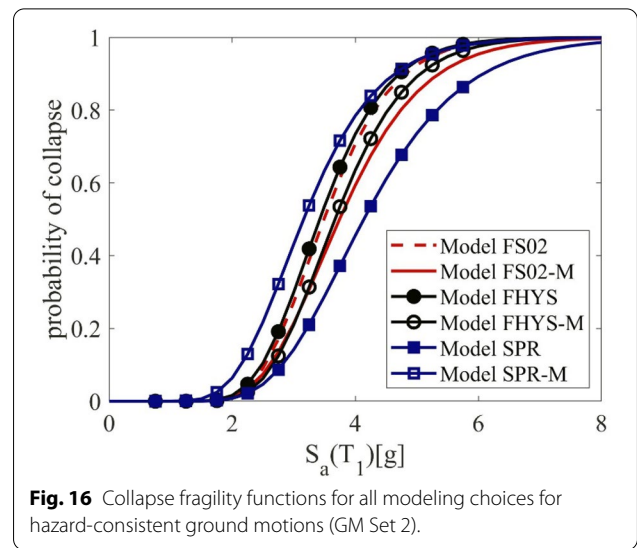


Fig. 16 Collapse fragility functions for all modeling choices for hazard-consistent ground motions (GM Set 2).

modeling options. The resulting collapse fragility functions are shown in Fig. 16—in this case modeling choices are seen to have a more significant effect on the median collapse probability which varies between $S_a = 3.18$ g to $S_a = 4.12$ g. The least conservative estimate of the collapse probability is obtained with model SPR; however, the most conservative estimate occurs with the same model with imposed failure constraints (as was the case with the IDA study).

It is also observed that using hazard consistent motions (GM Set 2) results in less conservative estimates of the collapse probability of the building. Considering the median probability of collapse, the required spectral

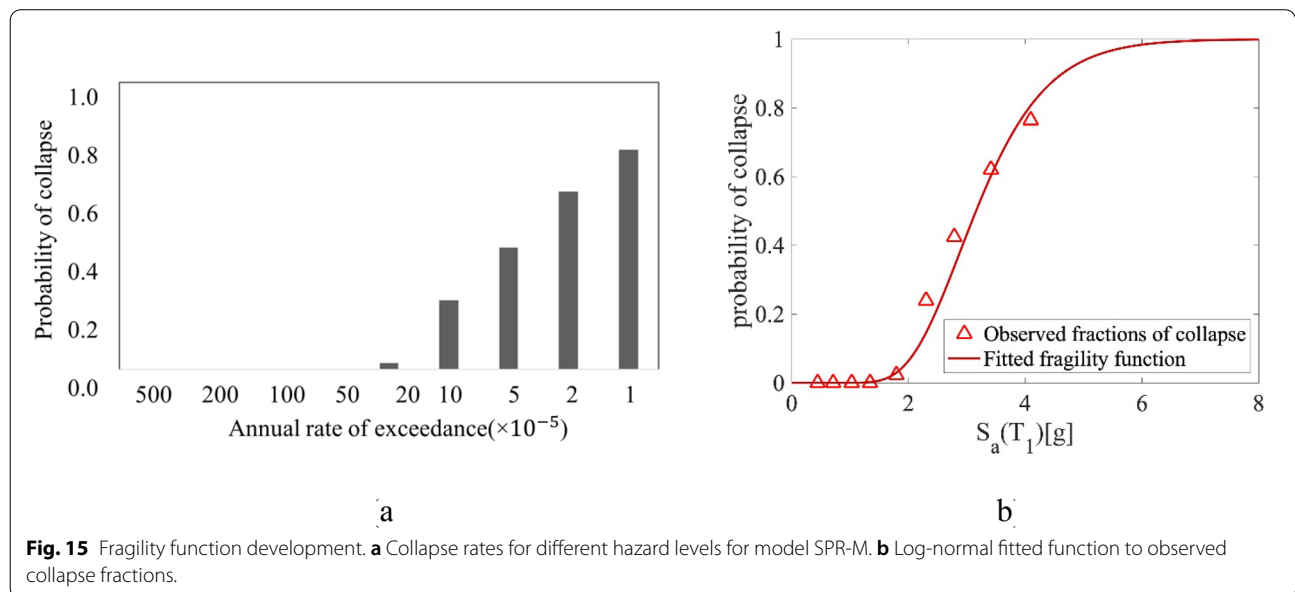


Fig. 15 Fragility function development. **a** Collapse rates for different hazard levels for model SPR-M. **b** Log-normal fitted function to observed collapse fractions.

Table 4 Variation in intensity measure (g) for different collapse probabilities.

Method	$P_{collapse} = 0.1$		$P_{collapse} = 0.5$		$P_{collapse} = 0.9$	
	Min	Max	Min	Max	Min	Max
IDA	1.44	1.72	2.50	2.85	4.05	5.20
CSS	2.05	2.80	3.18	4.12	4.71	6.15

demand ($S_a(T_1)$) for GM Set 2 compared to GM Set 1 increases from 2.7 g to 3.5 g (30%) for model FS02 and from 2.5 g to 3.0 g (20%) for model SPR-M. A summary of the collapse probabilities corresponding to 10%, 50% and 90%, highlighting the minimum and maximum IMs among all six models, is displayed in Table 4.

Finally, the results of the simulations are utilized to examine the risk associated with different seismic demands. Given the MIDR for each ground motion set and using the associated rates of each time series, the EDP hazard can be obtained using

$$\lambda(\text{EDP}) \equiv \nu(\text{EDP} > d) = \sum_{i=1}^{\text{\#records}} \text{Rate}_i H(\text{MIDR} - d), \tag{11}$$

where $\lambda(\text{EDP}) \equiv \nu(\text{EDP} > d)$ is the annual frequency with which the engineering demand parameter or EDP (the maximum interstory drift, in this case) d is exceeded, Rate_i is the rate of GM_i and $H(\text{MIDR} - d)$ is the Heaviside function that is assigned a value of 0 or 1 depending on whether the MIDR for a particular time series i exceeds a certain drift d . Figure 17 shows the resulting hazard curves for both GM selection methods as well as all modeling options considered in the study. The horizontal lines in the figures indicate the drift demand for a design level event with a 10% probability of being exceeded in 50 years (i.e., a return period of 474 years) varies between 1.8 and 2.1% using IDA and GM Set 1, whereas it reduces to 1.3–1.6% for the different modeling options when hazard-consistent motions are used (CSS approach). The return period at the code-mandated drift limit of 2% ranges from 830 to 1160 years for the CSS-based motions but reduces significantly to 450–510 years for GM Set 1. This implies that the current ASCE 7-16 guidelines for limiting maximum interstory drifts to 2% for design level events with a 10% probability of being exceeded in 50 years is conservative if hazard-consistent motions are used in the assessment, whereas the drift limitation appears to be justified when using IDA and GM Set 1.

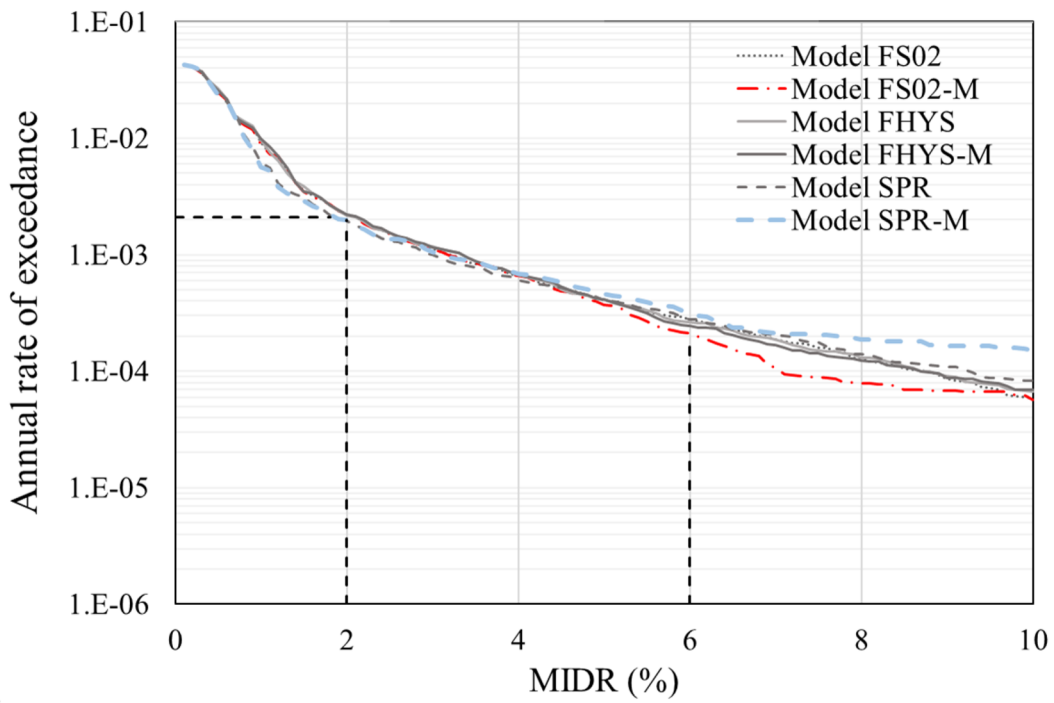
Finally, considering the collapse limit state, the return period varies between 3100 years (model SPR-M)—4700 years (model FS02-M) for GM Set 1 with IDA, but the range changes drastically to 12,000 years

(model SPR-M)—40,000 years (model SPR) when the CSS approach is used. This is a significant discrepancy that highlights the impact of GM selection on collapse probability.

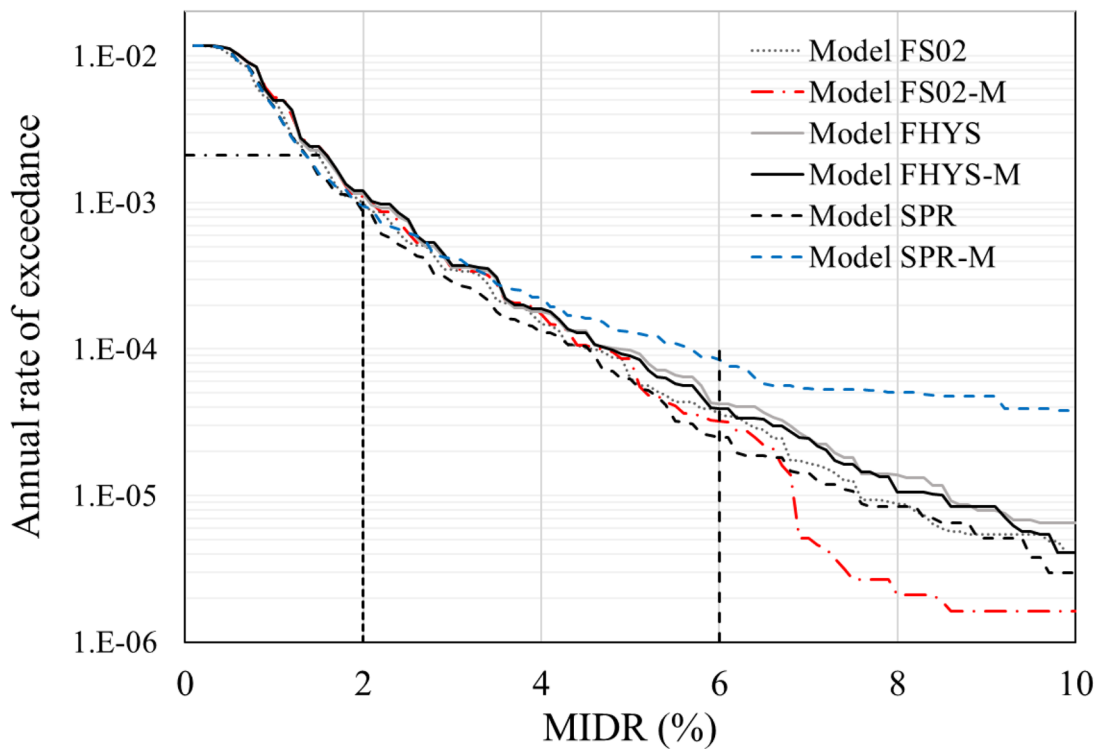
7 Conclusion

The effects of ground motion selection and choice of element and material modeling parameters on establishing collapse fragility functions and assessing demand risk were evaluated for a mid-rise code-compliant RC building. Findings from the study indicate that GM selection plays a more significant role than modeling considerations on the predicted collapse probabilities and collapse risk. The CSS approach, which is an enhancement of the Conditional Spectra (CS) method incorporating spectra with assigned rates of occurrence that reproduce the hazard at the site over a period range, resulted in lower collapse probabilities than IDA, where the selected GMs were based on site characteristics (soil type and fault distance) and an additional criterion for the composition of pulse-like motions in the GM set. The variability in the median collapse probability across all modeling options was less significant for the IDA than the CSS approach. In both cases though, the building model with phenomenological concentrated plasticity springs with embedded failure constraints (SPR-M) produced the most conservative estimate of collapse probability.

The study also examined the annual risk associated with a maximum interstory drift, providing a means to assess the true return period corresponding to target drifts, such as the ASCE 7-16 mandated interstory drift limit or an extreme limit corresponding to imminent collapse, as well as the variability in the risk for different modeling options. The IDA study suggests that the code-mandated story drift limit of 2% represents a reasonable design requirement for the return period associated with the design event, whereas the use of hazard-consistent motions indicate the requirement to be overly conservative. In general, using the CSS approach resulted in less conservative estimates—both in terms of demand and collapse risk. However, considering the importance of using hazard-consistent motions, the CSS methodology is recommended for seismic assessment of structures. It should also be emphasized that the findings reported in this paper are based on the assessment of a single



a IDA methodology



b CSS approach

Fig. 17 Hazard curves for maximum interstory drift.

building and additional studies on buildings of varying height and different plan configurations will be needed to make general recommendations. But the general methodology utilized in the present study can be extended to other building types and to investigate the effects of additional modeling parameters and GM selection methods.

Acknowledgements

The authors appreciate the advice and assistance of Norman Abrahamson on GM selection and for providing access to the computer code for the selection of ground motions for the CSS approach.

Authors' contributions

JZ carried out all the simulations, processed the results and assisted in drafting the original manuscript. ZZ assisted in the design of the building and in carrying out some of the simulations. TW was responsible for generating the CSS motions and assisting in the risk calculations. SK conceived the study and drafted the initial and final version of the manuscript. All authors read and approved the final manuscript.

Author's information

JZ (Graduate Student Researcher at University of California, Davis); ZZ (Graduate Student Researcher at University of California, Davis), TW (Graduate Student Researcher at University of California, Berkeley), SKK (Distinguished Professor at University of California, Davis).

Funding

Partial financial assistance provided by the University of California (Davis and Berkeley) to support the graduate studies of Jin Zhou, Zhelun Zhang and Tessa Williams is gratefully acknowledged.

Availability of data and materials

The datasets used or analyzed during the current study are available from the corresponding author on reasonable request.

Declarations

Competing interests

The authors declare that they have no competing interests.

Author details

¹Civil and Environmental Engineering, University of California, Davis, CA 95616, USA. ²Civil and Environmental Engineering, University of California, Berkeley, CA 94720, USA.

Received: 17 February 2021 Accepted: 13 April 2021

Published online: 26 May 2021

References

- Arteta, C. A., & Abrahamson, N. A. (2019). Conditional scenario spectra (CSS) for hazard-consistent analysis of engineering systems. *Earthquake Spectra*, *35*(2), 737–757.
- ASCE. (2005). *Minimum design loads for buildings and other structures*. ASCE 7–05, Reston, VA: ASCE
- ASCE/SEI. (2016). *Minimum design loads and associated criteria for buildings and other structures*. ASCE 7-16, American Society of Civil Engineers, Reston, VA
- ACI (American Concrete Institute). (2014). *Building Code Requirements for Structural Concrete (ACI 318-14) and Commentary*. ACI 318R, Farmington Hills, MI: ACI
- Baker, J. W. (2011). Conditional mean spectrum: tool for ground-motion selection. *Journal of Structural Engineering*, *137*(3), 322–331. [https://doi.org/10.1061/\(ASCE\)St.1943-541x.0000215](https://doi.org/10.1061/(ASCE)St.1943-541x.0000215)
- Baker, J. W., & Cornell, C. A. (2005). A vector-valued ground motion intensity measure consisting of spectral acceleration and epsilon. *Earthquake Engineering and Structural Dynamics*, *34*, 1193–1217
- Bertero, V. (1980). Strength and deformation capacities of buildings under extreme environments. *Structural engineering and structural mechanics*, A Volume Honoring Edgar P. Popov, K. Pister, ed., Prentice-Hall, Englewood Cliffs, N.J., pp. 188–237
- Davalos, H., & Miranda, E. (2019). Evaluation of bias on the probability of collapse from amplitude scaling using spectral shape matched records. *Earthquake Engineering and Structural Dynamics*, *48*(8), 970–986. <https://doi.org/10.1002/eqe.3172>
- Haselton, C. B., Liel, A. B., Deierlein, G. G., Dean, B. S., & Chou, J. H. (2011). Seismic collapse safety of reinforced concrete buildings. I: Assessment of ductile moment frames. *Journal of the Structural Engineering. American Society of Civil Engineers*, *137*(4), 481–491
- Ibarra, L., & Krawinkler, H. (2005). *Global collapse of frame structures under seismic excitations*. Report No. PEER 2005/06, Pacific Earthquake Engineering Research Center, University of California at Berkeley, Berkeley, CA
- Ibarra, L., & Krawinkler, H. (2011). Variance of collapse capacity of SDOF systems under earthquake excitations. *Earthquake Engineering and Structural Dynamics*, *40*, 1299–1314
- Iervolino, I., Maddaloni, G., & Cosenza, E. (2008). Eurocode 8 compliant real record sets for seismic analysis of structures. *Journal of Earthquake Engineering*, *12*(1), 54–90. <https://doi.org/10.1080/13632460701457173>
- Jalayer, F. (2003). Direct probabilistic seismic analysis: implementing non-linear dynamic assessments. Ph.D. Thesis, Dept. of Civil and Environmental Engineering, Stanford University, Stanford, CA
- Jalayer, F., & Cornell, C. A. (2009). Alternative non-linear demand estimation methods for probability-based seismic assessments. *Earthquake Engineering and Structural Dynamics*, *38*, 951–972. <https://doi.org/10.1002/eqe.876>
- Koopae, M., Dhakal, R., & MacRae, G. (2015). Analytical simulation of seismic collapse of RC frame buildings. *Bulletin of the New Zealand Society for Earthquake Engineering*, *48*(3), 157–169
- Koopae, M., Dhakal, R., & MacRae, G. (2017). Effect of ground motion selection methods on seismic collapse fragility of RC frame buildings. *Earthquake Engineering and Structural Dynamics*, *46*(11), 1875–1892
- Liel, A. B., Haselton, C. B., & Deierlein, G. G. (2011). Seismic collapse safety of reinforced concrete buildings. II: Comparative assessment of nonductile and ductile moment frames. *Journal of the Structural Engineering. American Society of Civil Engineers*, *137*(4), 492–502
- Lee, K., & Foutch, D. A. (2002). Performance evaluation of new steel frame buildings for seismic loads. *Earthquake Engineering and Structural Dynamics*, *31*(3), 653–670
- Lin, T., & Baker, J. (2015). Conditional spectra. In M. Beer, I. A. Kougioumtzoglou, E. Patelli, & I.S.-K. Au (Eds.), *Encyclopedia of earthquake engineering*. (p. 13). Berlin: Springer.
- Luco, N., & Cornell, C. A. (2007). Structure-specific scalar intensity measures for near-source and ordinary earthquake ground motions. *Earthquake Spectra*, *23*(2), 357–392
- Menegotto, M., & Pinto P.E. (1972). *Method of analysis for cyclically loaded R.C. frames including changes in geometry and non-elastic behavior of elements under combined normal force and bending*. Report 32, Istituto di Scienza e Tecnica delle Costruzioni, University of Rome, Italy
- OpenSees. (2019). Open system for earthquake engineering simulation. <http://opensees.berkeley.edu>. Pacific Earthquake Engineering Research Center, University of California, Berkeley
- Rajeev, P., & Tesfamariam, S. (2012). Seismic fragilities for reinforced concrete buildings with consideration of irregularities. *Structural Safety*, *39*, 1–13
- Scott, B. D., Park, R., & Priestley, M. J. N. (1982). Stress-strain behavior of concrete confined by overlapping hoops at low and high strain rates. *ACI Journal*, *79*(1), 13–27
- Shome, N., & Cornell, C.A. (1999). Probabilistic seismic demand analysis of nonlinear structures. *RMS-35. RMS Program*, Stanford, CA, 320
- Shome, N., Cornell, C. A., Bazzurro, P., & Carballo, J. E. (1998). Earthquakes, records, and nonlinear responses. *Earthquake Spectra*, *14*, 469–500
- Vamvatisikos, D., & Cornell, C. A. (2002). Incremental dynamic analysis. *Earthquake Engineering and Structural Dynamics*, *31*, 491–514
- Yassin, M.H.M. (1994). Nonlinear analysis of prestressed concrete structures under monotonic and cycling loads. PhD dissertation, University of California, Berkeley.

Publisher's Note

Springer Nature remains neutral with regard to jurisdictional claims in published maps and institutional affiliations.